OPEN ACCESS

Orbitally driven behaviour: Mott transition, quantum oscillations and colossal magnetoresistance in bilayered $Ca_3Ru_2O_7$

New Journal of Physics
The open–access journal for physics

Orbitally driven behaviour: Mott transition, quantum oscillations and colossal magnetoresistance in bilayered $Ca_3Ru_2O_7$

G Cao[1], X N Lin[1], L Balicas[2], S Chikara[1], J E Crow[2,3] and P Schlottmann[2,3]

[1] Department of Physics and Astronomy, University of Kentucky, Lexington, KY 40506, USA
[2] National High Magnetic Field Laboratory, Tallahassee, FL 32310, USA
[3] Department of Physics, Florida State University, Tallahassee, FL 32306, USA
E-mail: cao@uky.edu

New Journal of Physics **6** (2004) 159
Received 26 July 2004
Published 5 November 2004
Online at http://www.njp.org/
doi:10.1088/1367-2630/6/1/159

Abstract. We report recent transport and thermodynamic experiments over a wide range of temperatures for the Mott-like system $Ca_3Ru_2O_7$ at high magnetic fields, B ($\leqslant 30$ T). This work reveals a rich and highly anisotropic phase diagram, where applying B along the a-, b-, and c-axis leads to vastly different behaviour. A fully spin-polarized state via a first-order metamagnetic transition is obtained for $B \geqslant 6$ T and $B \| a$, and colossal magnetoresistance is seen for $B \| b$, and quantum oscillations in the resistivity are observed for $B \| c$, respectively. The interplay of the lattice, orbital and spin degrees of freedom are believed to give rise to this strongly anisotropic behaviour.

PII: S1367-2630(04)83925-9

Contents

1. Introduction

The ruthenates belong to a class of new materials of highly correlated electrons that is rich in novel physical properties. It has become increasingly clear that in the ruthenates the orbital degrees of freedom play a fundamental role. The phenomena are driven by the coupling of the orbits to the spin (spin–orbit interaction) and to the lattice (Jahn–Teller effect). The central feature of the 4d-electron-based materials is their extended orbitals, which lead to comparable and hence competing energies for the crystalline fields, Hund's rule interactions, spin–orbit coupling, p–d hybridization and electron-lattice coupling. The Ru ions are surrounded by six O-atoms forming RuO_6 octahedra. Crystallographic distortions and the relative orientation of the octahedra and their tilting are believed to determine the exotic properties of $Ca_3Ru_2O_7$ and other ruthenates.

The bilayered $Ca_3Ru_2O_7$ features a Mott-like transition, a metamagnetic transition [1, 2], colossal magneto-resistance and quantum oscillations in the resistivity [3]–[5]. Due to the strong crystalline field anisotropies, the coupling of the magnetic field to the system crucially depends on the orientation of the field relative to the crystal axis. This is evidence for the importance of the orbital degrees of freedom in this system and other ruthenates. The Shubnikov–de Haas oscillations along with other measurements for fields along the c-axis confirm the existence of a well-defined Fermi surface (FS) with closed orbits in the ab-plane [3]. The poor metallic behaviour of the $Ca_3Ru_2O_7$ system observed in the transport properties is then a consequence of the low carrier density and partial gapping of the FS.

For temperatures below 56 K and small magnetic fields the magnetic properties of $Ca_3Ru_2O_7$ are consistent with antiferromagnetic long-range order. The ordered magnetic moments lie in the ab-plane, but the details of the relative spin orientations is not yet established. When the temperature is lowered to 48 K, a discontinuous transition leads to a new state with a partially gapped Fermi surface. The first-order transition manifests itself in the magnetization, specific heat, the lattice parameter along the c-axis, the resistivity and the Raman scattering spectrum. We speculate that this new phase has both, antiferromagnetic and orbital, long-range order and that the charge gap of 0.1 eV observed by Raman spectroscopy [6, 7] is due to the orbital order rather than of the Mott-type.

As a function of field, a metamagnetic transition is observed when a field of 6 T is applied along the a-axis. For fields larger than 6 T the spins are ferromagnetically aligned with an ordered

moment of $1.73\mu_B$/Ru, approaching the anticipated full moment for Ru^{4+} ($S = 1$). The transition is also accompanied by a colossal magnetoresistive effect. The ferromagnetic alignment of the spin gives rise to a reduction in the resistivity by one order of magnitude. The physics is very different if the magnetic field is applied along the *b*- or *c*-axis.

In this paper, we present the experimental evidence for a yet incomplete phase diagram. In section 2 we show magnetization and resistivity measurements as a function of temperature and a wide range of magnetic fields ($0 \leqslant B \leqslant 30$ T) applied along the *a*-, *b*- and *c*-axis. The results are discussed in section 3 in an attempt to provide a coherent picture for the bilayer $Ca_3Ru_2O_7$. It is now clear that the lattice, orbital and spin degrees of freedom are intimately coupled to each other. A brief summary is given in section 4. Techniques of crystal growth and characterization are described in an appendix.

2. Results

The bilayered $Ca_3Ru_2O_7$ is the second member of the Ruddlesden–Popper series with room-temperature lattice parameters of $a = 5.3720(6)$ Å, $b = 5.5305(6)$ Å and $c = 19.572(2)$ Å [2]. The crystal structure is severely distorted by tilting of the RuO_6 octahedra. The tilt projects primarily onto the *ac*-plane (153.22°), while it only slightly affects the *bc*-plane (172.0°) [2]. These are crucial bond angles determining the crystalline field splitting of the 4d-orbitals and the overlap matrix elements between orbitals within the basal plane. They directly impact the band structure and are the origin for the anisotropic properties of the compound. $Ca_3Ru_2O_7$ displays antiferromagnetic (AFM) long-range order below $T_N = 56$ K while remaining metallic [1], and then at $T_{MI} = 48$ K it undergoes a partial Mott-like transition [1]–[10]. This partial Mott transition is associated with a significant reduction in the conductivity for $T < T_{MI}$ and the formation of a charge gap of 0.1 eV [6, 7] in one of the bands, while the system still remains a poor metal.

Shown in figure 1(a) is the temperature dependence of the magnetization, $M(T)$, for a field of $B = 0.5$ T applied along the *a*-, *b*- and *c*-axis (left scale) together with the temperature dependence of the lattice parameter of the *c*-axis (right scale). $M(T)$ for the three orientations at $B \geqslant 6.5$ T is presented in figure 1(b). The magnetization strongly depends on the orientation of the magnetic field. There are two major features that are critically linked to later discussions.

Firstly, the low field $M(T)$ for the *a*-axis, the magnetic easy axis, shows two phase transitions, $T_N = 56$ K and $T_{MI} = 48$ K. In contrast, $M(T)$ for the *b*-axis exhibits no discernable anomaly corresponding to T_{MI} but a sharp peak at T_N as seen in figure 1(a). For the *c*-axis, the two transitions are observed but considerably weakened. In addition, the precipitous decrease of M for the *a*-axis at T_{MI} when T is lowered is accompanied by a simultaneous sudden reduction in the *c*-axis lattice parameter. Hence, there is substantial magnetoelastic coupling that leads to Jahn–Teller distortions of the RuO_6 octahedra and their relative orientations [2, 3].

Secondly, as B applied parallel to the *a*-axis increases, T_{MI} shifts slightly downward, whereas T_N remains initially essentially unchanged and eventually becomes rounded off at higher fields. For $B \geqslant 6$ T, the magnetic state is driven to a *spin-polarized or ferromagnetic* (FM) state. In contrast, when B is parallel to the *b*-axis, T_N decreases with increasing B approximately at a rate of $2K/T$. Remarkably, the magnetic ground state for $B \| b$-axis *remains antiferromagnetic*, entirely different from that for $B \| a$-axis (see figure 1(b)). Unlike the *a*- and *b*-axis magnetization, the

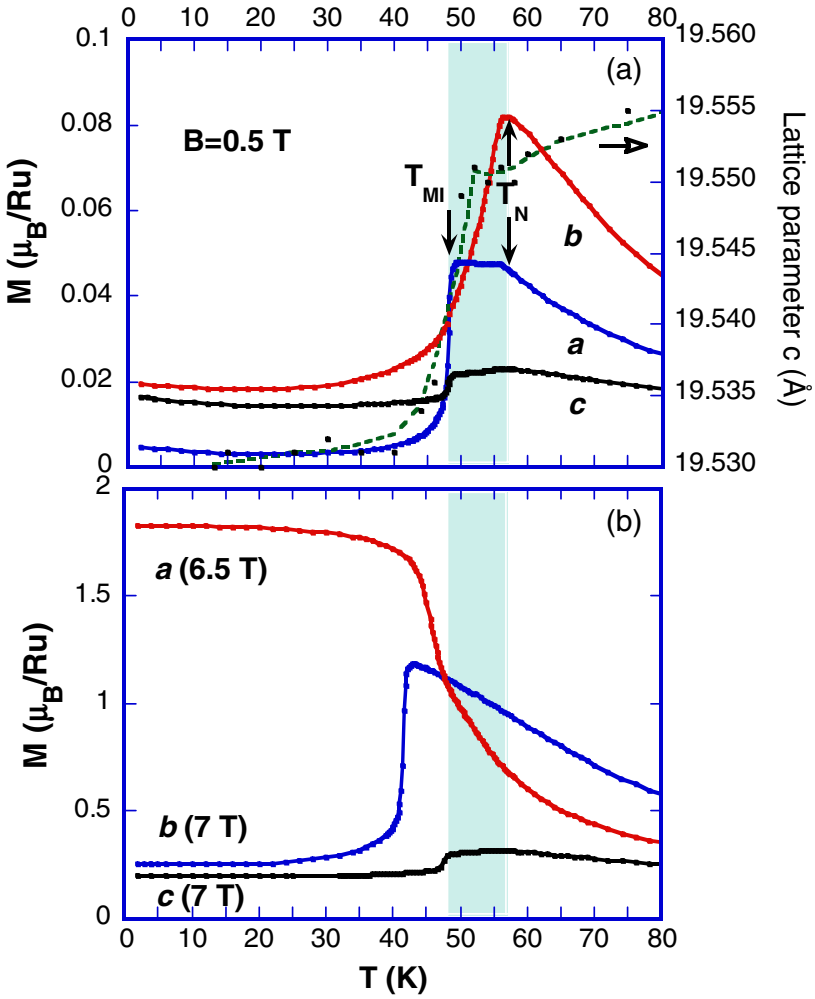

Figure 1. Temperature dependence of magnetization, M, for the field along the a-, b- and c-axis for (a) $B = 0.5\,\mathrm{T}$ and (b) $B > 6.5\,\mathrm{T}$. The lattice parameter of the c-axis (right-hand scale) versus temperature is also shown in (a). The shaded area highlights the region between T_{MI} and T_{N}.

c-axis magnetization remains essentially unchanged. This suggests that intraplane spin couplings are particularly strong.

The anisotropy of the magnetic state is further illustrated in figure 2 showing the isothermal magnetization at $T = 5\,\mathrm{K}$. It displays the first-order metamagnetic transition at $B = 6\,\mathrm{T}$ leading to the spin-polarized or ferromagnetic state with a saturation moment $M_{\mathrm{s}} = 1.73\mu_{\mathrm{B}}/\mathrm{Ru}$ when B is applied along the a-axis. Hence, more than 85% of the hypothetical saturation magnetization of $2\mu_{\mathrm{B}}/\mathrm{Ru}$ expected for an $S = 1$ system is achieved. The behaviour is completely different if the field is applied along the b- or c-axis, in part due to a strong anisotropy field of 22.4 T [10].

Figures 3(a) and (b) show the resistivity for the current along the c- and a-axis, ρ_{c} and ρ_{a}, respectively, as a function of B for $B\|a$-, b- and c-axis at $T = 0.6\,\mathrm{K}$. Both, ρ_{c} and ρ_{a}, drastically depend on the orientation of the field. This anisotropy and the coupling of the spin, orbital and lattice degrees of freedom are a central finding of this work. In the case of $B\|a$-axis (*magnetic*

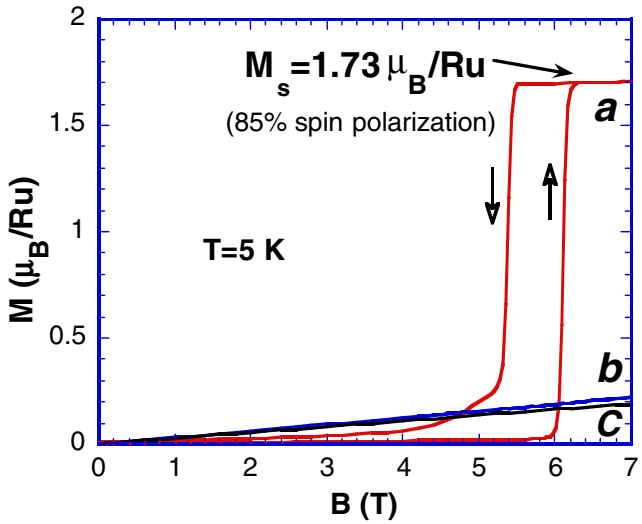

Figure 2. Isothermal magnetization M for $B\|a$-, b- and c-axis at $T = 5$ K. Note that the magnetic easy-axis is along the a-axis (with metamagnetic transition) with a high-field spin polarization of more than 85%.

easy-axis) for $T < 42$ K, both ρ_a and ρ_c show an abrupt drop by an order of magnitude at 6 T, which corresponds to the first-order metamagnetic transition leading to the spin-polarized state with more than 85% polarized spins as shown in figure 2. Further increases in B up to 30 T only result in a weak linear dependence of the resistivity with B. In contrast, for $B\|b$-axis (*magnetic hard axis*) for $T < 42$ K where the magnetic state remains antiferromagnetic, ρ_c and ρ_a rapidly decrease by as much as two and three orders of magnitude, respectively, at a critical field of $B_c = 15$ T (B_c decreases with increasing temperature). For $B\|c$-axis, both ρ_c and ρ_a show Shubnikov–de Haas oscillations corresponding to very small cross-sections of the Fermi surface.

It is clear that the transport properties strongly depend on the magnitude and orientation of the magnetic field. Such anisotropic coupling of the field to the system is only conceivable via orbital degrees of freedom coupled via the spin–orbit interaction to the spin of the 4d-electrons. It also requires that the degeneracy of the t_{2g}orbitals be lifted by deformations of the RuO_6 octahedra. In particular, the tilting angle of the octahedral provides a sensitive coupling to the lattice. Hence, spin, orbital and lattice degrees of freedom are intimately coupled with each other. A coupling of the resistivity and magnetization is clearly reflected known in colossal magnetoresistive (CMR) materials such as the manganites [11, 12], and this mechanism could explain the metal–insulator transition for $B\|a$. But the physics in $Ca_3Ru_2O_7$ is more complex from that driving other magnetoresistive materials, where a spin-polarized state is essential for CMR [12]. This is evidenced in figure 3 with the strong decrease in the resistivity for $B\|b$, while the magnetization is small and proportional to the field (see figure 2). The question is then, *what is the origin of the abrupt reduction in the resistivity by as much as three orders of magnitude when $B\|b$-axis*? Below we address this issue with more detailed results.

2.1. Colossal magnetoresistance

The temperature dependence of ρ_c with $B\|a$-axis is shown in figure 4(a) and $B\|b$-axis in figure 4(b) for a few representative values of B. (Note that the same log scale is used in both

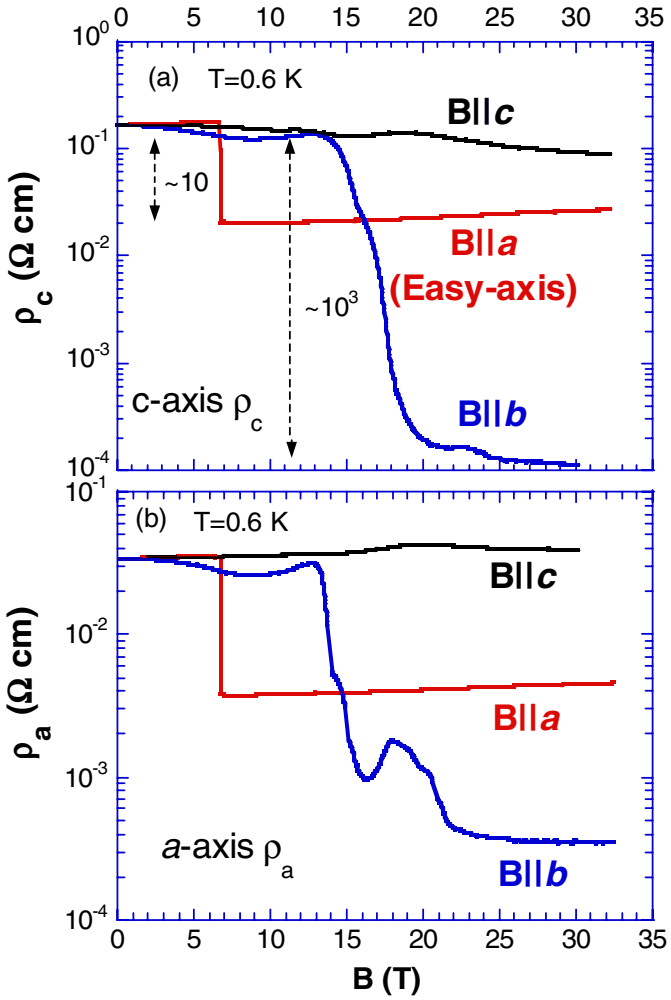

Figure 3. Magnetic field dependence of the resistivity for the current along the a- and c-axis, ρ_c (a) and ρ_a (b), respectively, for $B\|a$-, b- and c-axis at $T = 0.6$ K.

panels to facilitate comparison.) ρ_a displays the same temperature dependence for $B\|a$- and b-axis, and is therefore not shown here. For $B\|a$-axis, at low temperatures, ρ_c increases slightly with increasing B when $B < 6$ T, and decreases abruptly by about an order of magnitude when $B \geqslant 6$ T, at which the first-order metamagnetic transition leads to the spin-polarized state as seen in figures 2 and 3. A further increase in B results in a slightly higher resistivity at low temperatures. ρ_c corresponds to the coherent motion of electrons between Ru–O planes separated by insulating (I) Ca–O planes. A reduction in ρ_c in high fields is attributed to a field-induced enhancement of the tunnelling between the planes due to the spin polarization. This situation is similar to an array of FM/I/FM junctions or spin filters where the probability of tunnelling and thus the electronic conductivity depends on the angle between the spin magnetization of adjacent ferromagnets. For $Ca_3Ru_2O_7$, the spin-polarized state still does not generate a fully metallic state in spite of the pronounced reduction in ρ_c. In fact, the ρ_c at $B = 28$ T is still that of a bad metal or low carrier density system (see the inset). In sharp contrast, when $B\|b$-axis, the magnetic hard axis for $T < 42$ K, the temperature of the sharp discontinuity in ρ_c decreases approximately at a rate

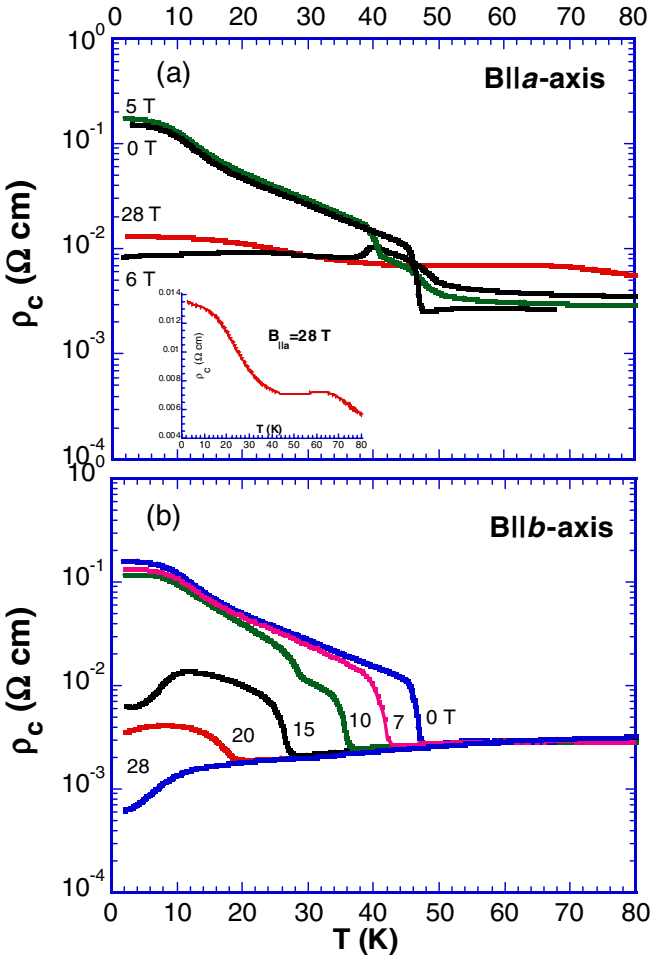

Figure 4. Temperature dependence of the resistivity for the current along the c-axis, ρ_c, at a few representative B up to 28 T applied along (a) the a-axis and (b) the b-axis for $1.2\,\mathrm{K} < T < 80$. Inset: ρ_c versus T for $B\|a = 28\,\mathrm{T}$. The temperature dependence of the a-axis resistivity ρ_a is very similar to that of ρ_c presented here and is therefore not shown.

of $2K/T$, and disappears for $B > 24\,\mathrm{T}$, as seen in figure 4(b). Again, these results suggest a strong magneto-orbital coupling.

2.2. *Rotation of easy axis*

As shown in figure 5, in the vicinity of T_{MI} ($42 \leqslant T \leqslant 48\,\mathrm{K}$), the magnetic easy-axis starts to rotate away from the a-axis and becomes parallel to the b-axis close to T_{MI} with the saturation moment M_s being only $0.8\mu_B$/Ru at $B = 6.2\,\mathrm{T}$. Here the angle θ is defined as the angle between B and the a-axis and the applied field is of 6.2 T. This rotation of the easy axis is driven by the change in the c-axis lattice parameter with temperature shown in figure 1. Between T_{MI} and T_{N} (the shaded area in figure 1) the ferromagnetism no longer favours the a-axis, but the b-axis. Hence, the magnetic states below T_{MI} and between T_{MI} and T_{N} evolve out of a different antiferromagnetically ordered state.

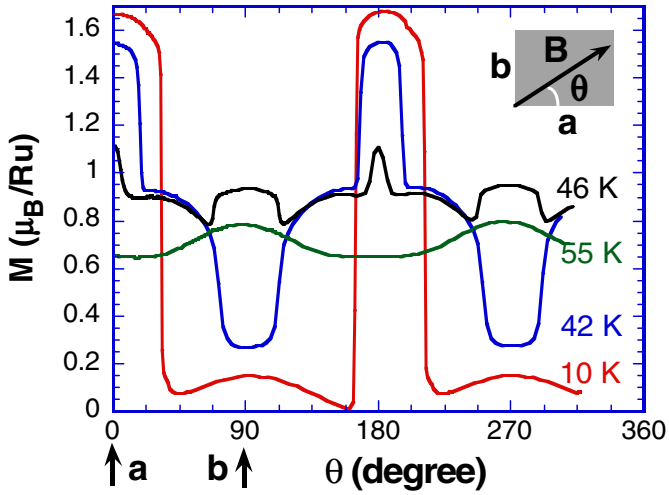

Figure 5. M as a function of angle, θ, between the a-axis and B at $B = 6.2$ T for the temperatures indicated. $\theta = 0$ corresponds to B along the a-axis. Note that M decreases abruptly when B rotates away from the a-axis for $T < 40$ K and that the easy-axis starts to rotate to the b-axis ($\theta = 90^\circ$) with increasing temperature when $T > 42$ K.

2.3. Quantum oscillations ($B \| c$-axis)

When B is applied along the c-axis, the quantum oscillations are observed in both ρ_a and ρ_c for 20 mK $< T <$ 6.5 K. Illustrated in figure 6(a) is ρ_c as a function of B (ρ_a is not shown). The amplitude of the quantum oscillations as a function of inverse field B^{-1} is presented in figures 6(b) and (c) for ρ_c and ρ_a, respectively. Quantum oscillations are a trademark of a Fermi liquid with closed orbits and long mean free path. The Shubnikov–de Haas oscillations are found for the $B \| c$-axis, but no quantum oscillations are discerned for the $B \| a$- or b-axis. Hence, they must be associated with the motion of the electrons in the a–b planes.

The analyses of the oscillations for ρ_c reveal an extremely low frequency $f_1 = 28$ T, which, based on crystallographic data [2] and the Onsager relation $F_0 = A(h/4\pi^2 e)$ (where e is the electron charge and h is Planck's constant), corresponds to an area of only 0.2% of the first Brillouin zone. Shown in figure 6(b) as the thin lines is the beating between two frequencies ($f_1 = 28$ T and $f_2 = 10$ T). The same analyses for ρ_a yields a slightly higher frequency of 33 T as shown in figure 6(c). The similar frequencies estimated from both ρ_a and ρ_c imply that the same orbitals may be responsible for the quantum oscillations. The cyclotronic effective mass is estimated to be $\mu_c = 0.85 \pm 0.05$. It is markedly smaller than the enhanced thermodynamic effective mass ($\sim$3) estimated from the electronic contribution, γ, to the specific heat [5]. There are two possible sources for this discrepancy: (1) The cyclotronic effective mass is measured in a relatively large magnetic field that quenches correlations, while the specific heat is a zero-field measurement, and (2) μ_c only refers to one closed orbit, while the thermodynamic effective mass measures an average over the entire Fermi surface.

In figure 7, we present ρ_c as a function of B at low temperature for the field pointing slightly away from the c-axis (within the ac-plane). As discussed before, a field component along the

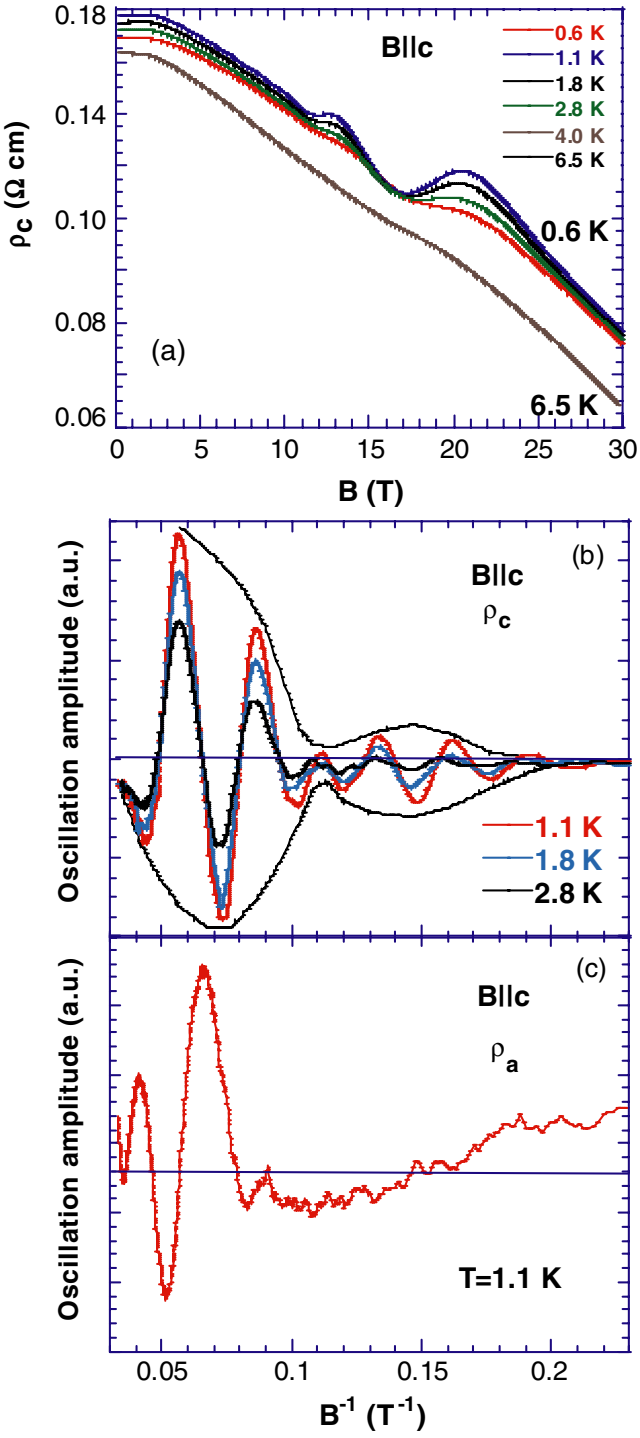

Figure 6. (a) Magnetic field dependence of ρ_c for $B\|c$-axis for a few representative temperatures as indicated (ρ_a is not shown); (b) the amplitude of the quantum oscillations (QOs) as a function of inverse field B^{-1} for ρ_c; (c) the amplitude of the QOs as a function of inverse field B^{-1} for ρ_a. The field dependence of the a-axis resistivity ρ_a is very similar to that of ρ_c presented here.

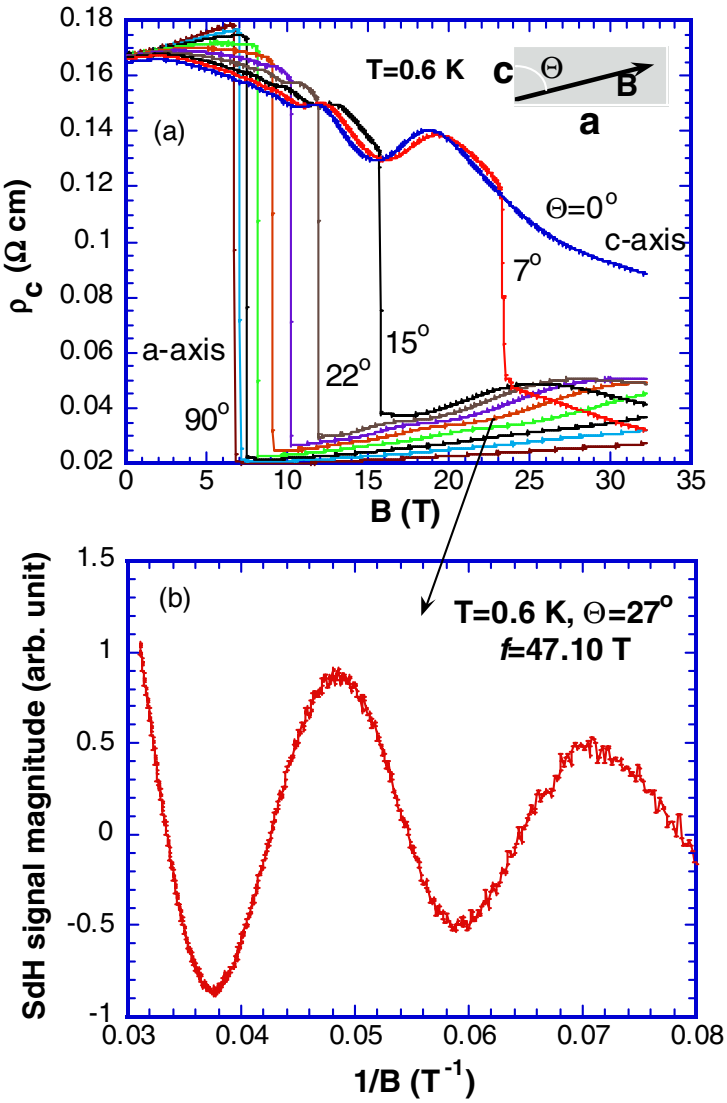

Figure 7. (a) Magnetic field dependence of ρ_c (for B within the ac-plane) for various orientations, Θ, defined as the angle between B and the c-axis; (b) the amplitude of the quantum oscillations (QOs) as a function of inverse field B^{-1} at $\Theta = 27^\circ$.

a-axis induces the first-order metamagnetic transition. If Θ is now the angle the field forms with the c-axis, then for $\Theta = 90^\circ$ ($B \| a$) the transition occurs at 6 T, but for smaller Θ, or as B rotates closer to the c-axis, the transition occurs at a larger field. From the previous discussion we expect to see Shubnikov–de Haas oscillations for fields less than the field of the transition. However, the oscillations persist for fields above the critical field, but with a larger frequency of $\sim$47 T for $\Theta = 27^\circ$ as shown in figure 7(b). In contrast, surprisingly, no oscillations are discerned for B in the bc-plane.

Note that the oscillation signature decreases with increasing angle and, as shown in figure 7, the quantum oscillations disappear when $\Theta > 45^\circ$, i.e. for the quantum oscillations

to occur, the angle between B and the c-axis should not be larger than 45°. This suggests that for small Θ the cross-section of the closed orbit is slightly enhanced due to the tilting of the direction of the field, but the Fermi surface is otherwise not drastically modified. However, with increasing Θ, the effect of the field on the Fermi surface is more significant and closed orbits disappear; they are possibly replaced by open ones, which do not contribute to quantum oscillations.

3. Discussion

The unusual and novel behaviour observed in the ruthenate $Ca_3Ru_2O_7$ is predominantly associated with the role of the orbital degrees of freedom and their coupling to the electron spin and the lattice. The orbital degeneracy of the 4d levels is lifted by the crystalline field splitting arising in first place by the RuO_6 octahedra. In a first approximation, the two e_g levels are split off from the three t_{2g} orbitals. The Hund's rule energy maximizing the total spin at each Ru site is not large enough to overcome the e_g–t_{2g} splitting, so that the e_g levels are not populated and can be disregarded for all practical purposes. Hence, one t_{2g} orbital is doubly occupied, while the other two host a single electron each. The octahedra are deformed (all lattice parameters are different) and consequently the three t_{2g} levels are expected to have different energies. These splittings are believed to be larger than the thermal energy k_BT and the Zeeman effect.

The octahedra are corner-shared and tilted, with a larger tilting angle in the ac-plane than in the bc-plane. The tilting plays a fundamental role for the hybridization matrix elements between states corresponding to neighbouring octahedra. Small changes in the tilting can give rise to qualitative changes in the properties. In view of the strong crystalline field and tilting angle asymmetries, the coupling of the magnetic field to the system depends on the orientation of the field. In other words, the matrix elements for the orbital Zeeman effect depend on the direction of the field. Consequently, different properties can be expected if the field is applied along the a-, b- or c-axis.

As shown in figure 1(a), for a small magnetic field, the system is paramagnetic at high temperatures and undergoes a transition to an antiferromagnetic state at $T_N = 57$ K. The ordered magnetic moment lies in the a–b plane and appears to be oriented along the a-axis. A magnetic field of about 6 T along the a-axis flops the spins of one of the antiferromagnetic sublattices leading to a ferromagnetic state. No such reorientation effect is observed if the field is applied along the b- or c-axis.

Also shown in figure 1(a) is an abrupt decrease in the c-axis lattice parameter at T_{MI} as the temperature is lowered. This change in the lattice parameter is accompanied by a decrease in the magnetization for the field applied along the a- and c- direction (but not along b) and an increase in the resistivity ρ_c. The transition temperature T_{MI} decreases with increasing field if the field is applied along the b-axis. A Raman-scattering study of $Ca_3Ru_2O_7$ revealed that the transition at T_{MI} is associated with the opening of a charge gap, $\Delta_c \sim 0.1$ eV, and the concomitant softening and broadening of an out of phase O phonon mode. This is indicative of a rearrangement in the t_{2g} orbitals, possibly either with a change in the Jahn–Teller distortions, a buckling of Ru–O–Ru bonds or the onset of long-range orbital ordering. The interpretation in terms of orbital order is particularly appealing because of the decrease in T_{MI} with field. Loosely speaking, due to the antisymmetry of the wavefunction, spin ferromagnetism tends to be accompanied by antiferro-orbital order. Orbital ordering in single layered ruthenates has been predicted theoretically [13, 14] and was suggested from x-ray data [15].

The observed metal–insulator transition is only a partial one, because the compound remains a poor metal below T_{MI}. Poor metallic behaviour can arise either from a low carrier density or a short mean free path. The observation of Shubnikov–de Haas oscillations at low temperatures is a clear indication of a well-established Fermi surface with closed orbits and a sufficiently long mean-free path of the carriers. The orbits correspond to very small cross-sections of the Fermi surface (less than 1% of the Brillouin zone cross-section). Hence, they must be associated with small electron or hole pockets and the system should be characterized as a low carrier-density compound.

The first-order antiferromagnetic to ferromagnetic metamagnetic transition as function of magnetic field, when a field of 6 T is applied along the *a*-axis, is also clearly seen as a drop in the resistivity. This transition resembles that of systems displaying colossal magnetoresistance. In the antiferromagnetic state the transport along the *c*-axis is reduced due to the fact that the spins of the layers are not aligned at $B = 0$. The spin-filter effect then prevents the carriers to tunnel through the layers. In a sufficiently strong magnetic field (along the *a*-direction) the spins are reoriented ferromagnetically and coherent motion of the electrons can again take place.

The electronic band structure and magnetism of $Sr_3Ru_2O_7$ have been investigated using the local density approximation (LDA) and the linearized augmented plane wave method by Singh and Mazin [16]. The Sr-based compound is expected to have some common aspects with the Ca-bilayer system. The calculation was carried out in the idealized tetragonal symmetry and in the experimental orthorhombic structure. The d_{xy} orbitals give rise to a cylindrical electron-like sheet centred about the Γ and Z points with weak dispersion along the *c*-direction, because of the rather small interplanar coupling. The d_{xz} and d_{yz} orbitals, on the other hand, provide flat sheet-like sections with strong nesting. Nesting could be responsible for the antiferromagnetic long-range order or antiferro-orbital order. The Fermi surface within the LDA calculations is found to be very sensitive to small structural changes and shifts in the Fermi energy.

For the single-layer ruthenate $Ca_{2-x}Sr_xRuO_4$, an orbital-selective Mott metal–insulator transition has been predicted [14]. This theoretical study (based on band structure calculations using the LDA, LDA + U and the dynamical mean-field approximation methods) explains the insulating and metallic phases with a coexistence of localized and itinerant orbitals, respectively. The metal–insulator transition observed as a function of *x* is attributed to a crossover of crystalline field levels and the concomitant localization/delocalization of 4d orbitals. The orbital-selective Mott-transition mechanism has been questioned by a very detailed model calculation for a two-band Hubbard system [17]. A different explanation for the transitions in the single layer system [18] is based on a cooperative occupation of the d_{xy} orbitals and their ferro-orbital ordering. The charge gap observed in the bilayer $Ca_3Ru_2O_7$ [6, 7] may not arise from a Mott metal–insulator transition. The possible mechanisms for its origin are a crystalline field level rearrangement due to coupling to phonons (Jahn–Teller distortion), a buckling of Ru–O–Ru bonds or antiferro-orbital order. The latter is the most likely scenario. Further investigations with microscopic probes are necessary to gain deeper insight into this issue.

4. Summary

As summarized in figure 8, $Ca_3Ru_2O_7$ displays a rich and complex phase diagram. The distortions and tilting of the RuO_6 octahedra give rise to highly anisotropic magnetic and orbital properties. We have presented evidence that in this compound the spin, orbital and lattice degrees of freedom

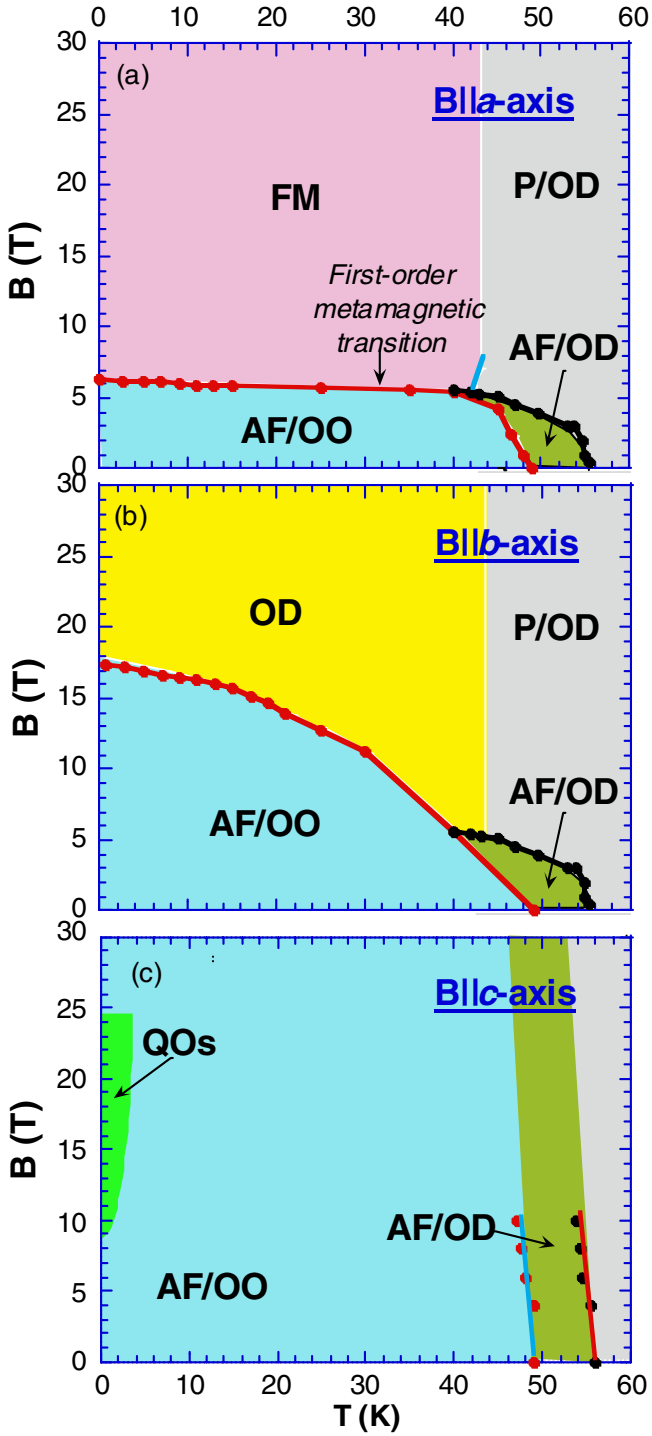

Figure 8. Phase diagram plotted as B versus T summarizing various phases for (a) $B\|a$-axis, (b) $B\|b$-axis and (c) $B\|c$-axis. OO, orbital order; OD, orbital disorder; QO, quantum oscillations; P, paramagnetism; AF, antiferromagnetism.

are intimately coupled. As a consequence of the anisotropies in the lattice structure, applying the magnetic field B along the a-, b- and c-axis leads to very different properties.

Two transitions are observed in the magnetization: resistivity and the lattice parameter of the c-axis when the applied field is small. The high-temperature phase is paramagnetic and without orbital order. Below T_N the system orders antiferromagnetically, where the detailed orientation of the ordered moments is not yet known. Below the second transition at T_{MI}, a charge gap opens, which could be associated with the onset of antiferro-orbital order. A magnetic field reduces the two transition temperatures.

If a field of 6 T is applied along the a-axis, the system undergoes a first-order metamagnetic transition into a ferromagnetic state. Here the antiferromagnetic order is broken up by the field. It is not clear if the orbital order persists. With increasing T there is a gradual crossover into the paramagnetic/orbitally disordered state. If, on the other hand, the magnetic field is applied along the b-axis, an abrupt transition into a metallic state occurs at a much larger field. The transition could be associated with the breakdown of the long-range orbital order. Finally, when the field is oriented along the c-axis, Shubnikov–de Haas oscillations are found at low temperatures. These oscillations correspond to closed orbits in the ab-plane with small cross-section. The large resistivity of the system is attributed to a low carrier density.

Acknowledgments

GC is grateful to Dr Zhong Fang for very helpful discussions. The work was supported by NSF grant no. DMR-0240813 along with the National High Magnetic Field Laboratory through NSF Cooperative Agreement DMR-0084173 and the State of Florida. PS acknowledges the support by NSF (grant no. DMR01-05431) and DOE (grant no. DE-FG02-98ER45707).

Appendix

The flux growth method has been used for single-crystal growth of the ruthenates studied. Single crystals of $Ca_3Ru_2O_7$ were grown in Pt crucibles from off-stoichiometric quantities of RuO_2, $CaCO_3$ and $CaCl_2$ mixtures with $CaCl_2$ being self flux. The Ca : Ru and $CaCO_3$: $CaCl_2$ ratio in the mixture was approximately 7 : 1 and 1 : 12, respectively. The mixtures were first heated to 1500 °C in a Pt crucible covered by a Pt cover, soaked for 25 h, and slowly cooled at 2–3 °C h^{-1} to 1350 °C and finally cooled to room temperature at 100 h^{-1}. The starting Ca : Ru ratio and the thermal treatments are critical and subtle for formation of $Ca_3Ru_2O_7$ crystals as nucleation of its sister compounds $CaRuO_3$ and $Ca_2RuO_4$are more energetically favourable. By carefully changing the ratio and thermal treatments, we have successfully grown crystals of $Ca_{n+1}Ru_nO_{3n+1}$ and $Sr_{n+1}Ru_nO_{3n+1}$ with $n = 1, 2, 3$ and ∞. Single crystals of $Ca_3Ru_2O_7$ are plate-like with the c-axis along the short dimension. We used Lindberg box furnaces which provide high-temperature stability critical for the crystal growth.

The crystals studied were characterized by single-crystal x-ray diffraction, Laue x-ray diffraction, SEM and TEM. All results indicate that the single crystals studied are of high quality. This is consistent with highly anisotropic physical properties and low Dingle temperature (<3 K) observed in $Ca_3Ru_2O_7$. The magnetically easy-axis was determined to be along the a-axis based on magnetic measurements on crystals whose crystallographic axes were already identified by TEM. $Ca_3Ru_2O_7$ provides two unique advantages for us to identify the a- and b-axis: (1) the first-order metamagnetic transition only occurs sharply at 6 T along the a-axis; hence one can

easily align the *a*-axis with magnetic field by measuring the onset of the metamagnetic transition (see figure 2); (2) the *b*-axis magnetic susceptibility shows no anomaly at 48 K; hence one can then readily determine the *b*-axis by measuring temperature dependence of magnetic susceptibility (see figure 1). We also use this feature to identify twinned crystals which often show a small kink at 48 K in the *b*-axis susceptibility. Rotating probes were used for both resistivity and magnetic measurements in high fields. These probes were driven by automated step motors with uncertainty less than 2°.

References

[1] Cao G, McCall S, Crow J E and Guertin R P 1997 *Phys. Rev. Lett*. **78** 1751
[2] Cao G, Abbound K, McCall S, Crow J E and Guertin R P 2000 *Phys. Rev.* B **62** 998
[3] Cao G, Balicas L, Xin Y, Dagotto E, Crow J E, Nelson C S and Agterberg D F 2003 *Phys. Rev.* B **67** 060406 (R)
[4] Cao G, Balicas L, Xin Y, Crow J E and Nelson C S 2003 *Phys. Rev.* B **67** 184405
[5] Cao G, Balicas L, Lin X N, Chikara S, Durairaj V, Elhami E, Brill J W, Rai R C and Crow J E 2004 *Phys. Rev.* B **69** 014404
[6] Liu H L, Yoon S, Cooper S L, Cao G and Crow J E 1999 *Phys. Rev.* B **60** R6980
[7] Snow C S, Cooper S L, Cao G, Crow J E, Nakatsuji S and Maeno Y 2002 *Phys. Rev. Lett.* **89** 226401
[8] Puchkov A V, Schabel M C, Basov D N, Startseva T, Cao G, Timusk T and Shen Z-X 1998 *Phys. Rev. Lett*. **81** 2747
[9] Guertin R P, Bolivar J, Cao G, McCall S and Crow J E 1998 *Solid State Commun*. **107** 263
[10] McCall S, Cao G and Crow J E 2003 *Phys. Rev.* B **67** 094427
[11] See, for example, Tsymbal E Y and Pettifor D G 2001 *Solid State Physics* vol 56, ed H Ehrenreich and F Spaepen (New York: Academic) p 113
[12] See, for example, Tokura Y 2000 *Colossal Magnetoresistive Oxides* (Sydney: Gordon and Beach)
[13] Hotta T and Dagotto E 2002 *Phys. Rev. Lett.* **88** 017201
[14] Anisimov V I, Nekrasov I A, Kondakov D E, Rice T M and Sigrist M 2002 *Eur. Phys. J.* B **25** 191
[15] Mizokawa T *et al* 2001 *Phys. Rev. Lett*. **87** 077202
[16] Singh D J and Mazin I I 2001 *Phys. Rev.* B **63** 165101
[17] Liebsch A 2003 *Phys. Rev. Lett*. **91** 226401
[18] Fang Z, Nagaosa N and Terakura K 2004 *Phys. Rev.* B **69** 045116